

Role of nonorthogonality of energy eigenstates in quantum systems with localized losses

Jan Wiersig*

Institut für Physik, Otto-von-Guericke-Universität Magdeburg, Postfach 4120, D-39016 Magdeburg, Germany

(Received 14 September 2018; published 6 November 2018)

The dynamics of a wave in an open quantum system can be described by the eigenstates of the non-Hermitian Hamiltonian, provided that it is not at an exceptional point. Naively, one would expect that the decay of the energy eigenstates directly determines the decay of the total wave intensity. We show, however, that this is not the case for systems with localized losses. Instead, the nonorthogonality of the energy eigenstates plays an important role. It can to a large extent compensate for the initial decay of the eigenstates leading to a transient power-law decay of the wave intensity with a potentially large exponent.

DOI: [10.1103/PhysRevA.98.052105](https://doi.org/10.1103/PhysRevA.98.052105)**I. INTRODUCTION**

The dynamics of open quantum and wave systems has attracted strong interest in recent years. Such an open system can often be described by an effective non-Hermitian Hamiltonian $\hat{\mathcal{H}}$. The non-Hermiticity of the Hamiltonian implies that its eigenvalues are in general complex, with the (negative) imaginary part being a decay rate. If the Hamiltonian is in addition non-normal, i.e., $[\hat{\mathcal{H}}, \hat{\mathcal{H}}^\dagger] \neq 0$, then its eigenstates are mutually nonorthogonal in general. The nonorthogonality becomes extreme near exceptional points (EPs) in parameter space [1–4], at which the eigenstates of the Hamiltonian fail to provide a basis for the Hilbert space. EPs have been experimentally observed in various systems, such as in microwave cavities [5], optical microcavities [6], coupled atom-cavity systems [7], photonic lattices [8], ultrasonic cavities [9], and exciton-polariton billiards [10]. There are a number of applications of EPs, ranging from sensors [11,12] to unidirectional lasing [13,14] and orbital angular momentum microlasers [15].

It is known that the nonorthogonality of energy eigenstates can lead to a nonexponential transient decay [16]. In optical systems with loss and gain, it has been discussed recently in the context of anomalous transient amplification [17]. Moreover, in parity-time symmetric optical systems the nonorthogonality of modes leads to an interesting interference effect called power oscillations [18,19]. The role of nonorthogonality and power oscillations in systems exhibiting parametric instability near EPs is discussed in Ref. [20]. The relation of nonorthogonality of energy eigenstates and the quantum-classical correspondence has been studied in Refs. [21–23]. A way to measure nonorthogonality by means of resonance-width shifts has been proposed in Ref. [24]. In lasers the nonorthogonality leads to quantum excess noise and therefore to an enhancement of the laser linewidth with respect to the Schawlow-Townes formula [25–30]. In perturbed or deformed microdisk cavities, nonorthogonality of optical modes is related to chirality, which refers to an unbalanced

contribution of clockwise- and counterclockwise-propagating waves [31,32].

The aim of the present paper is to uncover the role of nonorthogonality of energy eigenstates in the decay dynamics of waves subject to localized losses. In such a situation, which can be created, e.g., in optical systems [19], microwave systems [33], or Bose-Einstein condensates [34], a wave packet can travel a long time without attenuation before it encounters a lossy region. We show in a simple setup that the dynamics of the survival probability (or total wave intensity in the optical setting) is not reflected in the decay rates of the energy eigenstates but rather in their nonorthogonality properties.

This paper is organized as follows. The theory is introduced in Sec. II, beginning with the general setup in Sec. II A. The dynamics resulting from the time-evolution operator is discussed in Sec. II B and the dynamics in terms of the energy eigenstate expansion is discussed in Sec. II C. An upper bound for the wave intensity is derived and its dynamics is addressed in Sec. II D. Section III reports on numerical results for a simple example introduced in Sec. III A. The eigenvalues and eigenstates of the corresponding non-Hermitian Hamiltonian are calculated in Sec. III B. The wave dynamics is presented in Sec. III C, and the dynamics of the upper bound is presented in Sec. III D. Finally, a discussion and conclusions are given in Sec. IV.

II. THEORY**A. The general setup**

We consider an open quantum or wave system described by a state vector $|\psi\rangle$ in a Hilbert space of finite dimension N . The dynamics is determined by the Schrödinger equation

$$i \frac{d}{dt} |\psi\rangle = \hat{\mathcal{H}} |\psi\rangle, \quad (1)$$

where time is scaled such that $\hbar = 1$. The Hamiltonian $\hat{\mathcal{H}}$ is non-Hermitian due to the openness of the system. Schrödinger equations with effective Hamiltonians are used routinely, e.g., for the study of atomic and molecular dynamics [35], ultracold atoms in optical lattices [36,37], microwave cavities [38],

*jan.wiersig@ovgu.de

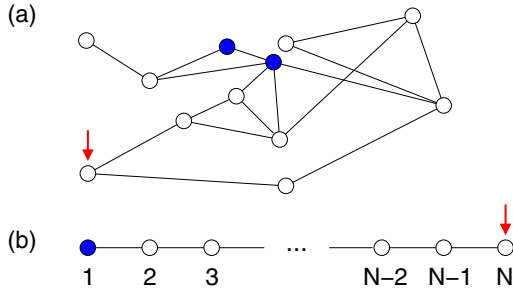


FIG. 1. Illustration of two undirected graphs which are associated with the discussed quantum systems. Vertices (circles) $j = 1, \dots, N$ are connected by undirected edges (lines) provided that the coupling matrix elements $\mathcal{H}_{jk} = \mathcal{H}_{kj}$ with $j \neq k$ are nonzero. Edges connecting a vertex to itself, i.e., loops, belong to \mathcal{H}_{jj} and are not shown. The solid circles mark vertices with losses and the arrow marks the position of an initial wave packet. (a) A generic example. (b) A linear graph.

electron transport in low-dimensional nanostructures [39], nuclear physics [40], and optical microcavities [32].

We restrict ourselves to systems which fulfill reciprocity. This implies that, in a basis $|1\rangle, \dots, |N\rangle$ invariant under time reversal, the Hamiltonian $\hat{\mathcal{H}}$ is a complex-symmetric matrix [38,41]. We can always choose \mathcal{H}_{jk} to be real for $j \neq k$ by using an appropriate orthogonal transformation. The quantity $\Gamma_j = -\text{Im}(\mathcal{H}_{jj}) \geq 0$ describes the loss at the basis state j . If $\Gamma_j = 0$ for most but not all of the basis states, then we say that the system has localized losses.

For our purpose it is convenient to associate with the quantum system introduced above an undirected finite graph with N vertices as illustrated in Fig. 1. Each vertex represents a vector of the above-discussed basis in Hilbert space. The vertex j is connected to vertex $k \neq j$ by an undirected edge if the matrix element $\mathcal{H}_{jk} = \mathcal{H}_{kj}$ is nonzero. Note that this mathematical representation is not related to quantum graphs studied in the field of quantum chaos [42]. As is usual in graph theory, we define the distance between two vertices as the number of edges in the shortest path connecting them.

With the discussed properties we can write the Hamiltonian also as

$$\hat{\mathcal{H}} = \hat{H}_0 - i\hat{\Gamma}, \quad (2)$$

where \hat{H}_0 is a real-symmetric matrix and $\hat{\Gamma}$ is a real diagonal matrix with nonnegative diagonal elements $\Gamma_1, \dots, \Gamma_N$. For nonempty graphs (hence, there is at least one edge) \hat{H}_0 is not diagonal. Together with $\hat{\Gamma}$ being diagonal it follows $[\hat{H}_0, \hat{\Gamma}] \neq 0$. This in turn implies $[\hat{\mathcal{H}}, \hat{\mathcal{H}}^\dagger] \neq 0$, i.e., $\hat{\mathcal{H}}$ is non-normal.

B. Dynamics: Application of the time-evolution operator

The time evolution of a state $|\psi(t)\rangle$ according to Eq. (1) is formally given by

$$|\psi(t)\rangle = \hat{G}(t)|\psi(0)\rangle, \quad (3)$$

with the initial state $|\psi(0)\rangle$ and the (nonunitary) time-evolution operator $\hat{G}(t) = e^{-i\hat{\mathcal{H}}t}$. Assume that the initial state is a wave packet localized on a single vertex (arrow in Fig. 1) which is connected to at least one of the lossy vertices (solid

circles in Fig. 1). If the minimal distance is $d > 1$ then this wave packet cannot start to decay immediately as it, roughly speaking, first has to find its way to the nearest lossy vertex. To derive a more precise statement, we first expand the formal solution (3):

$$|\psi(t)\rangle = \sum_{n=0}^{\infty} (-i)^n \frac{t^n}{n!} \hat{\mathcal{H}}^n |\psi(0)\rangle. \quad (4)$$

For the above-described situation the state $\hat{\mathcal{H}}^n |\psi(0)\rangle$ does not have an overlap with a lossy vertex for $n < d$. From this fact and the equation

$$\frac{d}{dt} \langle \psi(t) | \psi(t) \rangle = -2 \langle \psi(t) | \hat{\Gamma} | \psi(t) \rangle, \quad (5)$$

which can be easily derived from Eqs. (1)–(2), follows the important result for the dynamics of the total intensity:

$$\langle \psi(t) | \psi(t) \rangle = 1 + \alpha t^{2d+1} + O(t^{2d+2}), \quad (6)$$

i.e., the time evolution of the difference $1 - \langle \psi(t) | \psi(t) \rangle$ obeys a power law with an exponent $2d + 1$ determined by the distance d . The prefactor α is nonpositive and can be zero due to destructive interference. In such a special case the power law has an even larger exponent.

Note that a nonexponential decay itself is not surprising. Even in Hermitian systems, where a decay probability can be introduced as the overlap squared between time evolved and initial state, a transient square-law decay is expected as discussed in textbooks (see, e.g., Ref. [43]). This nonexponential decay plays an important role in the so-called quantum Zeno effect [44]. In our case, however, the exponent is potentially large, which results in a nearly attenuation-free propagation in the beginning followed by an abrupt decay of intensity.

Even though the decay of the total intensity (6) is extremely slow, it is nonzero even for arbitrarily small times. This can be interpreted as a consequence of the small tail that the wave packet develops.

C. Dynamics: Energy eigenstate expansion

Assuming that the system is not at an EP, we can expand any state $|\psi(t)\rangle$ in terms of the eigenstates $|\phi_j\rangle$ of the Hamiltonian

$$|\psi(t)\rangle = \sum_{j=1}^N a_j |\phi_j\rangle e^{-i\omega_j t}, \quad (7)$$

with the frequencies $\omega_j = E_j/\hbar$ and the energy eigenvalues E_j . The energy eigenstates are normalized in the conventional manner by $\langle \phi_j | \phi_j \rangle = 1$. The expansion coefficients $\vec{a} = (a_1, \dots, a_N)$ are chosen such that $|\psi(0)\rangle = |\psi_0\rangle$ with $\langle \psi_0 | \psi_0 \rangle = 1$. This is here done via $\vec{a} = V^{-1} \psi_0$ with the eigenvector matrix $V_{ij} = \langle i | \phi_j \rangle$ and $\psi_{0i} = \langle i | \psi_0 \rangle$. Alternatively, the last step could be formulated in a biorthogonal basis.

Since we want to describe a wave packet that decays on the long run, each term in the expansion (7) with $a_j \neq 0$ decays exponentially with the rate $\gamma_j = -\text{Im}\omega_j > 0$. This does, however, not imply that the total intensity $\langle \psi(t) | \psi(t) \rangle$ decays exponentially with the rate $2\gamma \in [\min 2\gamma_j, \max 2\gamma_j]$ as can be concluded from Eq. (6).

To see this also in the energy eigenstate expansion, we write the time-dependent total intensity of the state in Eq. (7) as

$$\langle \psi(t) | \psi(t) \rangle = \sum_{j,k=1}^N a_j^* U_{jk} a_k e^{-i(\omega_k - \omega_j^*)t}, \quad (8)$$

with the Bell-Steinberger nonorthogonality matrix [45]

$$U_{jk} = \langle \phi_j | \phi_k \rangle, \quad (9)$$

which is Hermitian and positive definite. Since a non-normal operator, like the Hamiltonian $\hat{\mathcal{H}}$, cannot be unitarily diagonalized, we have $\hat{U} \neq \mathbb{1}$, meaning that there is at least one nonorthogonal pair of eigenstates.

If all eigenstates were pairwise orthogonal, i.e., $U_{jk} = \delta_{jk}$, or if we would remove by hand all interference terms in Eq. (8), then the total intensity would consist only of diagonal terms such that

$$\langle \psi(t) | \psi(t) \rangle_{\text{dia}} = \sum_{j=1}^N |a_j|^2 e^{-2\gamma_j t}. \quad (10)$$

To get a deeper understanding of the role of the nondiagonal terms we expand the right-hand side of Eq. (8) as

$$\langle \psi(t) | \psi(t) \rangle = 1 + \sum_{n=1}^{\infty} f_n \frac{t^n}{n!}, \quad (11)$$

with real-valued coefficients

$$f_n = \sum_{j,k=1}^N a_j^* U_{jk} a_k [-i(\omega_k - \omega_j^*)]^n. \quad (12)$$

Comparing Eqs. (11) and (6) leads us to the conditions

$$f_n = 0 \quad \text{if } n < 2d + 1, \quad (13)$$

which, for a given initial wave, impose strong relations between the nonorthogonality matrix \hat{U} and the eigenfrequencies ω_j . Put another way, nonorthogonality and spectral properties conspire such that the dynamics in terms of the energy eigenstates is as given by the time-evolution operator.

D. Upper bound for the intensity

Following the idea in Ref. [17], we first derive a nontrivial upper bound for the total intensity $\langle \psi(t) | \psi(t) \rangle$. From Eq. (3) follows

$$\langle \psi(t) | \psi(t) \rangle = \langle \psi(0) | \hat{G}^\dagger(t) \hat{G}(t) | \psi(0) \rangle, \quad (14)$$

with the initial state $|\psi(0)\rangle$ normalized to unity. For given time t , the right-hand side of this equation is maximal if $|\psi(0)\rangle$ is the normalized eigenvector of the positive-definite Hermitian matrix $\hat{G}^\dagger(t) \hat{G}(t)$ with the largest eigenvalue, which is exactly the normalized right-singular vector of $\hat{G}(t)$ with the largest singular value $s_{\max}(t)$. The latter can be expressed by the spectral norm $\|\hat{G}(t)\| = s_{\max}(t)$. From this follows the upper bound for the total intensity:

$$\langle \psi(t) | \psi(t) \rangle \leq \|\hat{G}(t)\|^2. \quad (15)$$

The equality holds for a wave prepared initially to be the right-singular vector of $\hat{G}(t)$ corresponding to the largest singular

value. At time t it has the largest total intensity of all waves propagating in the system for a time t .

In contrast to Ref. [17] we restrict the class of possible Hamiltonians $\hat{\mathcal{H}}$ to those describing losses but no gains. In such a case \hat{G} is subunitary and therefore (see, e.g., Ref. [46])

$$\|\hat{G}(t)\| \leq 1. \quad (16)$$

From this upper bound, the asymptotic behavior in Eq. (6), and the upper bound for the total intensity in Eq. (15) follows

$$\|\hat{G}(t)\|^2 = 1 + \beta t^{2d_{\max}+1} + O(t^{2d_{\max}+2}), \quad (17)$$

with d_{\max} being at least as large as the maximum of the distances d for all initial conditions. β is a nonpositive coefficient. To conclude, also the dynamics of the upper bound $\|\hat{G}(t)\|^2$ shows a power-law behavior. This power law is, via Eq. (6), a consequence of the nonorthogonality of the energy eigenstates.

III. NUMERICAL RESULTS

A. The system

To keep the analysis as transparent as possible, the most simple example is considered, a linear chain of vertices $j = 1, \dots, N$ as illustrated in Fig. 1(b). The nearest-neighbor coupling $g > 0$ and the real-valued on-site energies are assumed to be uniform. With an appropriate gauge we can set the latter to zero. The loss is localized on the first vertex with the loss rate $\Gamma > 0$. The Hamiltonian is therefore

$$\hat{\mathcal{H}} = \begin{pmatrix} -i\Gamma & g & & & \\ g & 0 & g & & \\ & & \ddots & & \\ & & & g & 0 & g \\ & & & & g & 0 \end{pmatrix}, \quad (18)$$

where the matrix elements not shown are zero. Such a system could, e.g., be realized in optics by evanescent-field-coupled waveguides [19] or in microwave physics by evanescent-field-coupled dielectric resonators [33]. The system has been theoretically studied in the context of topological protection of coherence in Ref. [47], which is not related to the present topic.

The Hamiltonian (18) possesses a non-Hermitian particle-hole symmetry [48], also called charge-conjugation symmetry [49], which in the given basis is written as

$$\hat{\sigma} \hat{\mathcal{H}} \hat{\sigma} = -\hat{\mathcal{H}}^*, \quad (19)$$

with $\hat{\sigma}^2 = \mathbb{1}$ and the asterisk denotes complex conjugation. This symmetry implies that if $|\phi_j\rangle$ with components $\langle k | \phi_j \rangle$ is an eigenstate with the eigenvalue E_j , then $(\hat{\sigma} \phi_j)^*$ is an eigenstate with the eigenvalue $-E_j^*$. For the Hamiltonian (18) the operator $\hat{\sigma}$ is given by $\text{diag}(1, -1, 1, -1, \dots)$.

It is straightforwardly derived from the eigenvalue equation of the Hamiltonian (18) that

$$-\text{Im}(E_j) = |\langle 1 | \phi_j \rangle|^2 \Gamma, \quad (20)$$

i.e., the decay rate $-\text{Im}(E_j)$ of the given energy eigenstate $|\phi_j\rangle$ is determined by its overlap with the lossy vertex. This implies that a nondecaying eigenstate does not have an overlap with the lossy vertex. Such an eigenstate cannot exist as can be

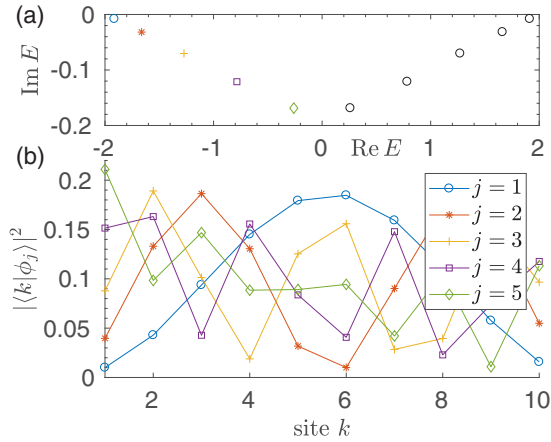


FIG. 2. (a) Complex energy eigenvalues of the linear chain with $N = 10$ vertices. The first vertex is subject to losses with the rate $\Gamma = 0.8$. Note that E and Γ are dimensionless since all energy scales are measured in units of the nearest-neighbor coupling g . (b) Absolute value squared of the components of the energy eigenstates $|\phi_j\rangle$ (also dimensionless) with $\text{Re}(E_j) \leq 0$. Lines are guides to the eye. According to the non-Hermitian particle-hole symmetry [Eq. (19)], the same picture results for the eigenstates with $\text{Re}(E_j) \geq 0$.

checked by inserting the nonzero vector $\vec{\phi} = (0, b_2, \dots, b_N)$ into the eigenvalue equation of the Hamiltonian (18).

In the following, all energy scales are measured in units of g . Time is then measured in units of \hbar/g . Without loss of generality, the two remaining parameters are fixed to $N = 10$ and $\Gamma = 0.8$.

B. Energy eigenvalues and eigenstates

A transcendental equation for the eigenvalues of the Hamiltonian (18) can be found in Ref. [47]. We, however, found it more convenient to directly compute the energy eigenvalues E_j and the eigenstates $|\phi_j\rangle$ using MATLAB. The solutions with $j = 1, \dots, N$ are sorted for increasing $\text{Re}(E_j)$. Figure 2(a) shows that the complex energy spectrum is symmetric with respect to the imaginary axis as predicted by the non-Hermitian particle-hole symmetry. The corresponding eigenstates are depicted in Fig. 2(b). As predicted by Eq. (20), the larger the overlap with the lossy vertex at $k = 1$ is, the larger the decay rate $-\text{Im}(E_j)$ is.

The nonorthogonality matrix is shown in Fig. 3. By virtue of the chosen normalization of the eigenstates, we have $U_{jj} = 1$. We can see that the elements $|U_{j \neq k}|$ are significantly large for small $|j - k|$ and that the values are larger the more lossy the involved eigenstates are (compare Fig. 2). The maximum off-diagonal element is $|U_{56}| = |U_{65}| \approx 0.5436$.

C. Time evolution

Figure 4 depicts the time evolution of the state $|\psi\rangle$ with the initial state $|\psi_0\rangle$ localized on the vertex on the far right-hand vertex, i.e., $\langle j|\psi_0\rangle = \delta_{jN}$. The distance to the lossy vertex is therefore $d = N - 1$. We can observe that the dynamics is rather trivial. Due to the immediate reflection at the last vertex $j = N$, the center of the wave packet first moves with constant velocity to the left. The width of the wave packet increases

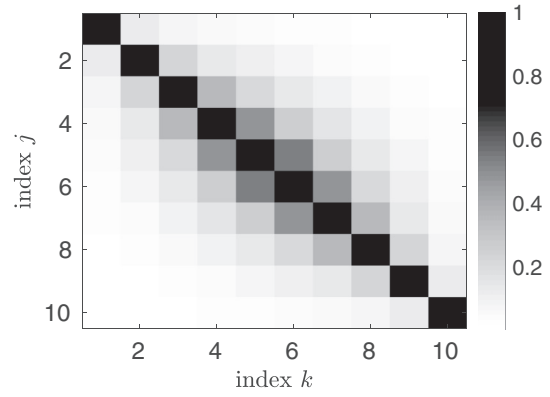


FIG. 3. The nonorthogonality matrix U_{jk} [Eq. (9)] for the linear chain. The absolute values of the dimensionless matrix elements are plotted in a grayscale representation: The maximum value of unity (corresponding to collinear states) is black and the minimum value of zero (orthogonal states) is shown in white.

slightly with time t . Around $t = 4.5$ the wave starts to overlap with the lossy vertex. For later times the wave has significantly decayed and partly backscattered.

The corresponding dynamics of the total intensity $\langle \psi(t)|\psi(t)\rangle$ of the wave packet is shown in Fig. 5. For a time until $t \leq 4.5$ the total intensity stays close to unity. Around $t = 4.5$ it starts to decay strongly because the wave packet has reached the lossy vertex. The data results from the eigenstate expansion in Eq. (8), which fully agrees with the results from a direct application of the time-evolution operator (3) (not shown). For comparison, the dashed curve shows the decay resulting from the diagonal terms only [setting \hat{U} to $\mathbb{1}$, see Eq. (10)]. Here, the decay of the total intensity sets in immediately after the time evolution starts, which proves that the nonorthogonality is essential for the description of the nonexponential transient decay of the total intensity in terms of energy eigenstates. Another unambiguous support of this claim is the dotted curve in Fig. 5 showing the decay of the longest-lived energy eigenstate. Even this slowest possible decay of an individual energy eigenstate is faster than the actual

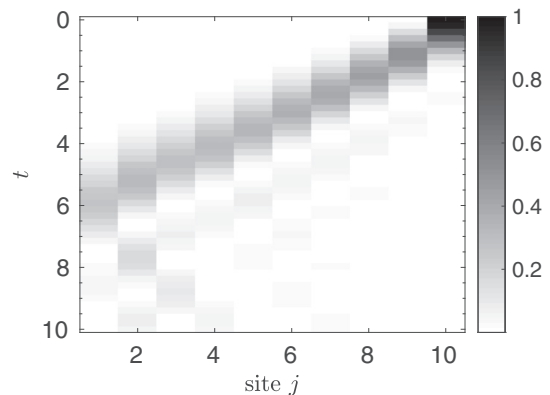


FIG. 4. Time evolution of a wave packet $|\psi(t)\rangle$ initially localized at the far right-hand vertex with $j = N = 10$. The intensity $|\langle j|\psi(t)\rangle|^2$ is shown in a grayscale representation; all quantities are dimensionless.

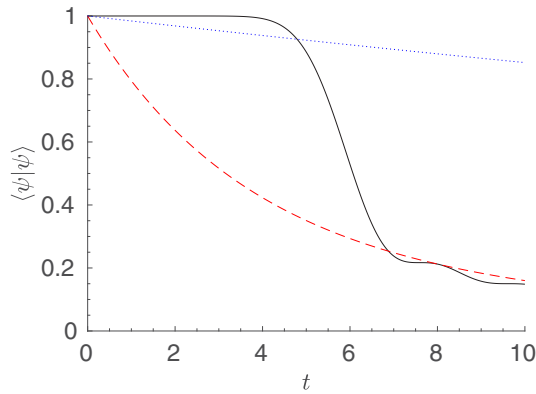


FIG. 5. The total intensity $\langle \psi(t) | \psi(t) \rangle$ of a wave packet initially localized at the site with $j = N = 10$ as a function of time t ; all quantities are dimensionless. The solid curve is the result of Eq. (8) (cf. Fig. 4) and the dashed curve is the result of Eq. (10) involving only the diagonal terms normalized to unity at $t = 0$. The dotted curve shows the decay of the longest-lived energy eigenstate.

decay of the wave packet. Of course, also the shorter-lived energy eigenstates contribute to the initial condition $\langle j | \psi_0 \rangle = \delta_{jN}$. In fact, there is approximately a uniform contribution of the energy eigenstates to the chosen initial state.

Figure 6 shows the difference $1 - \langle \psi(t) | \psi(t) \rangle$ on a double-logarithmic scale. In our numerical calculations this quantity is for small times constant $\approx 10^{-16}$ reflecting the machine precision of MATLAB. For times above this numerically inaccessible regime, $1 - \langle \psi(t) | \psi(t) \rangle$ is well fitted by the function αt^{2d+1} , where $d = N - 1 = 9$. This observation of a power law with such a remarkable large exponent confirms the prediction in Eq. (6). The deviations for larger times result from higher-order terms such as, e.g., the term proportional to t^{2d+2} .

The temporal expansion coefficient (12) is shown in Fig. 7. It can be seen that for $n < 2d + 1$ the coefficient is around 10 orders of magnitude smaller than that for $n \geq 2d + 1$. This is fully consistent with the conspiracy conditions (13). The fact that f_n is not exactly zero for $n < 2d + 1$ is again due to the finite machine precision.

D. Dynamics of the upper bound

To illustrate the dynamics of the upper bound, Fig. 8 compares the total intensity for different initial conditions

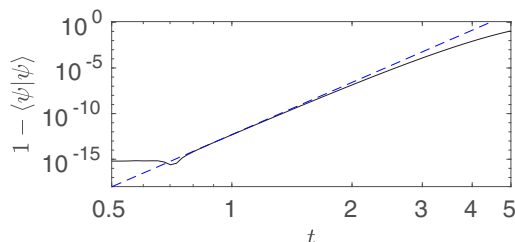


FIG. 6. The total intensity $\langle \psi(t) | \psi(t) \rangle$ relative to unity [solid curve, see Eq. (8)] as a function of time t in a double-logarithmic plot. As in Fig. 5 all quantities are dimensionless. The dashed line marks the function αt^{2d+1} , with $\alpha = 5 \times 10^{-13}$.

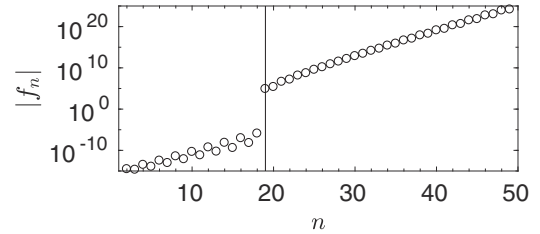


FIG. 7. The (dimensionless) temporal expansion coefficient f_n [Eq. (12)] of $\langle \psi(t) | \psi(t) \rangle$ with the initial condition $\langle j | \psi_0 \rangle = \delta_{jN}$ in a semilogarithmic plot. The vertical line marks the integer $n = 2d + 1$.

with the right-hand side of Eq. (15). It can be clearly seen that the latter stays close to unity for $t \leq 10$. The upper bound (15) is obeyed by the wave packet initially localized at the site with $j = N$ (dash-dotted curve) with a lifetime of around $t = 4.5$.

Longer-lived waves can be constructed according to the scheme explained in Sec. IID by using the right-singular vector with the largest singular value of the given time-evolution operator \hat{G} as the initial condition. The temporal behavior of such a wave prepared for $\hat{G}(8)$ is shown as dashed curve in Fig. 8. The total intensity of this wave stays close to unity for longer times around $t = 8.5$. Figure 9 reveals that this is possible because the wave first propagates to the right before it gets reflected and propagates to the left towards the lossy vertex. It should be pointed out that at $t = 0$ the wave is not localized at a single vertex but has a more complicated spatial structure. Note that a very small amount of the wave travels immediately to the left, which implies that for short times well below $t = 8.5$ the intensity decays slightly faster if compared to the wave packet initially localized at the site with $j = N$ (not shown).

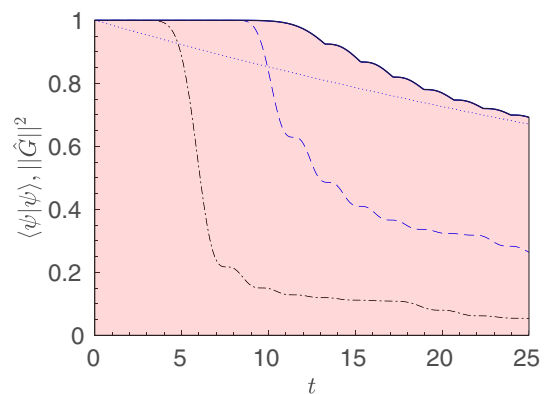


FIG. 8. The upper bound $\|\hat{G}(t)\|^2$ (solid curve) and the total intensity $\langle \psi(t) | \psi(t) \rangle$ corresponding to different initial conditions (dash-dotted, dashed, and dotted curves) at $t = 0$; both axes are dimensionless. All points in the shaded region satisfy the inequality (15). The dash-dotted curve showing the wave initially localized at the site with $j = N$ is the same as that in Fig. 5 but on a larger scale. The dashed curve shows the wave prepared initially to be the right-singular vector with the largest singular value of $\hat{G}(8)$. The decay of the longest-lived energy eigenstate is shown as a dotted curve.

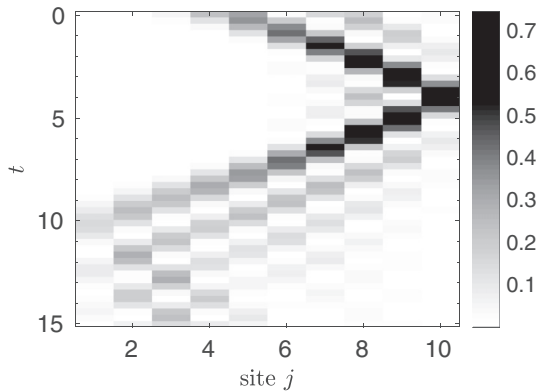


FIG. 9. Time evolution of a wave with initial conditions given by the right-singular vector with the largest singular value of $\hat{G}(8)$ (cf. Fig. 8). The intensity is shown in a grayscale representation. All quantities are dimensionless.

Figure 10 shows the departure of $\|\hat{G}\|^2$ from unity during time evolution. It can be observed that the numerical data are well fitted by $\beta t^{2d_{\max}+1}$, with $d_{\max} = d = N - 1$. This is fully consistent with the prediction in Eq. (17).

Note that for longer times the intensity of the energy eigenstate(s) with the smallest decay rate converges to the upper bound (see Fig. 8). Hence, for such long times the decay rate is determined simply by the decay of the longest-lived energy eigenstate(s). This is in contrast to the transient behavior where the nonorthogonality plays the decisive role.

IV. DISCUSSION AND CONCLUSIONS

We have studied the decay dynamics of waves in systems with localized losses. For a finite-dimensional system it has been shown that the nonorthogonality of energy eigenstates is necessary for a qualitative and quantitative description of the dynamics. We have derived the conspiracy conditions (13) for the nonorthogonality matrix and the energy eigenvalues depending on the initial wave packet. The consequence of these conditions is a transiently suppressed decay of the total intensity. The deviation from unity obeys a power law with an exponent given by the graph-theoretical distance d between the wave packet's initial vertex and the nearest lossy vertex.

We have validated our theory by means of numerical simulations on a simple example, a linear chain with a single lossy site, and found a very good agreement. Our numerical results demonstrate clearly that the nonorthogonality is playing a decisive role in explaining the decay dynamics. The

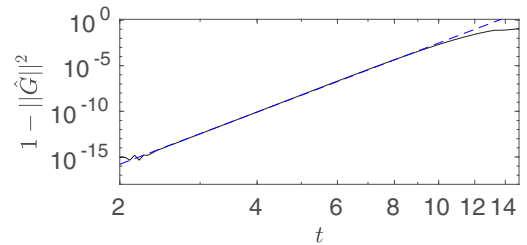


FIG. 10. The norm $\|\hat{G}\|^2$ squared relative to unity (solid curve) as a function of time t in a double-logarithmic plot (cf. Fig. 8). The dashed line marks the function $\beta t^{2d_{\max}+1}$, with $d_{\max} = d = N - 1$ and $\beta = 3 \times 10^{-22}$. All quantities are dimensionless.

qualitative results of our numerical study do not depend on the chosen values of the parameters.

We have checked that the results are robust against disorder (not shown) by introducing diagonal and off-diagonal disorder. In the latter case only nonzero elements are modified, keeping the distance d fixed.

In our systems loss can be replaced globally by gain simply by changing the sign of the imaginary parts of all the matrix elements of the Hamiltonian. This does not change the role of the nonorthogonality in the dynamics.

We have first considered the simplest case where the initial wave packet is restricted to a single site. This can be generalized to extended waves. The exponent $2d + 1$ is then only a lower bound as the waves may first escape from the nearest lossy site. We have studied a special class of extended waves given by the right-singular vector with the largest singular value of the time-evolution operator. These waves are the ones with the largest remaining intensity for a specified time.

The condition of reciprocity can be dropped by considering a directed graph. Here, the distance $d(a, b)$ between two vertices a and b is defined as the length of the shortest directed path from a to b which in general differs from $d(b, a)$.

Systems with localized losses are extreme cases. Other extreme cases are systems with uniform losses, where the decay dynamics in terms of energy eigenstates is trivial. In the more general case of nonuniform, but not necessarily localized, losses the importance of the nonorthogonality depends on the degree of nonuniformity. We expect therefore that the results presented in this paper are also relevant for the understanding of the dynamics of these more general non-Hermitian and non-normal systems.

ACKNOWLEDGMENTS

Fruitful discussions with H. Schomerus, L. Ge, K. G. Makris, J. Kullig, and M. Haque are acknowledged.

[1] T. Kato, *Perturbation Theory for Linear Operators* (Springer, New York, 1966).
 [2] W. D. Heiss, *Phys. Rev. E* **61**, 929 (2000).
 [3] M. V. Berry, *Czech. J. Phys.* **54**, 1039 (2004).
 [4] W. D. Heiss, *J. Phys. A* **37**, 2455 (2004).
 [5] C. Dembowski, H.-D. Gräf, H. L. Harney, A. Heine, W. D. Heiss, H. Rehfeld, and A. Richter, *Phys. Rev. Lett.* **86**, 787 (2001).

[6] S.-B. Lee, J. Yang, S. Moon, S.-Y. Lee, J.-B. Shim, S. W. Kim, J.-H. Lee, and K. An, *Phys. Rev. Lett.* **103**, 134101 (2009).
 [7] Y. Choi, S. Kang, S. Lim, W. Kim, J.-R. Kim, J.-H. Lee, and K. An, *Phys. Rev. Lett.* **104**, 153601 (2010).
 [8] A. Regensburger, C. Bersch, M.-A. Miri, G. Onishchukov, D. N. Christodoulides, and U. Peschel, *Nature (London)* **488**, 167 (2012).

- [9] Y. Shin, H. Kwak, S. Moon, S.-B. Lee, J. Yang, and K. An, *Sci. Rep.* **6**, 38826 (2016).
- [10] T. Gao, E. Estrecho, K. Y. Bliokh, T. C. H. Liev, M. D. Fraser, S. Brodbeck, K. M., C. Schneider, S. Höfling, Y. Yamamoto *et al.*, *Nature (London)* **526**, 554 (2015).
- [11] J. Wiersig, *Phys. Rev. Lett.* **112**, 203901 (2014).
- [12] W. Chen, Ş. K. Özdemir, G. Zhao, J. Wiersig, and L. Yang, *Nature (London)* **548**, 192 (2017).
- [13] B. Peng, Ş. K. Özdemir, M. Liertzer, W. Chen, J. Kramer, H. Yilmaz, J. Wiersig, S. Rotter, and L. Yang, *Proc. Natl. Acad. Sci. USA* **113**, 6845 (2016).
- [14] S.-S. Sui, Y.-Z. Huang, M.-Y. Tang, H.-Z. Weng, Y.-D. Yang, J.-L. Xiao, and Y. Du, *Opt. Lett.* **41**, 3928 (2016).
- [15] P. Miao, Z. Zhang, J. Sun, W. Walasik, S. Longhi, N. M. Litchinitser, and L. Feng, *Science* **353**, 464 (2016).
- [16] L. N. Trefethen and M. Embree, *Spectra and Pseudospectra* (Princeton University, Princeton, NJ, 2005).
- [17] K. G. Makris, L. Ge, and H. E. Türeci, *Phys. Rev. X* **4**, 041044 (2014).
- [18] K. G. Makris, R. El-Ganainy, D. N. Christodoulides, and Z. H. Musslimani, *Phys. Rev. Lett.* **100**, 103904 (2008).
- [19] C. E. Rüter, K. G. Makris, R. El-Ganainy, D. N. Christodoulides, M. Segev, and D. Kip, *Nat. Phys.* **6**, 192 (2010).
- [20] A. A. Zyablovsky, E. S. Andrianov, and A. A. Pukhov, *Sci. Rep.* **6**, 29709 (2016).
- [21] D. V. Savin and V. V. Sokolov, *Phys. Rev. E* **56**, R4911(R) (1997).
- [22] Y. V. Fyodorov and B. Mehlig, *Phys. Rev. E* **66**, 045202(R) (2002).
- [23] M. Kopp and H. Schomerus, *Phys. Rev. E* **81**, 026208 (2010).
- [24] Y. V. Fyodorov and D. V. Savin, *Phys. Rev. Lett.* **108**, 184101 (2012).
- [25] K. Petermann, *IEEE J. Quantum Electron.* **15**, 566 (1979).
- [26] A. E. Siegman, *Lasers* (University Science Books, Sausalito, CA, 1986).
- [27] H. Schomerus, K. M. Frahm, M. Patra, and C. W. J. Beenakker, *Phys. A (Amsterdam, Neth.)* **278**, 469 (2000).
- [28] H. Schomerus, *Phys. Rev. A* **79**, 061801(R) (2009).
- [29] Y. D. Chong and A. D. Stone, *Phys. Rev. Lett.* **109**, 063902 (2012).
- [30] J. C. Pillay, Y. Natsume, A. D. Stone, and Y. D. Chong, *Phys. Rev. A* **89**, 033840 (2014).
- [31] J. Wiersig, A. Eberspächer, J.-B. Shim, J.-W. Ryu, S. Shinohara, M. Hentschel, and H. Schomerus, *Phys. Rev. A* **84**, 023845 (2011).
- [32] J. Wiersig, *Phys. Rev. A* **84**, 063828 (2011).
- [33] C. Poli, M. Bellec, U. Kuhl, F. Mortessagne, and H. Schomerus, *Nat. Commun.* **6**, 6710 (2015).
- [34] G. Barontini, R. Labouvie, F. Stubenrauch, A. Vogler, V. Guarrera, and H. Ott, *Phys. Rev. Lett.* **110**, 035302 (2013).
- [35] W. P. Reinhardt, *Annu. Rev. Phys. Chem.* **33**, 223 (1982).
- [36] C. Keller, M. K. Oberthaler, R. Abfalterer, S. Bernet, J. Schmiedmayer, and A. Zeilinger, *Phys. Rev. Lett.* **79**, 3327 (1997).
- [37] M. V. Berry and D. H. J. O'Dell, *J. Phys. A* **31**, 2093 (1998).
- [38] H.-J. Stöckmann, E. Persson, Y.-H. Kim, M. Barth, U. Kuhl, and I. Rotter, *Phys. Rev. E* **65**, 066211 (2002).
- [39] G. L. Celardo and L. Kaplan, *Phys. Rev. B* **79**, 155108 (2009).
- [40] G. E. Mitchell, A. Richter, and H. A. Weidenmüller, *Rev. Mod. Phys.* **82**, 2845 (2010).
- [41] M. M. Sternheim and J. F. Walker, *Phys. Rev. C* **6**, 114 (1972).
- [42] T. Kottos and U. Smilansky, *Phys. Rev. Lett.* **79**, 4794 (1997).
- [43] L. E. Ballentine, *Quantum Mechanics: A Modern Development* (World Scientific, Singapore, 2010).
- [44] B. Misra and E. C. G. Sudarshan, *J. Math. Phys.* **18**, 756 (1977).
- [45] J. S. Bell and J. Steinberger, in *Proceedings, Oxford International Conference on Elementary Particles*, edited by R. G. Moorhouse, A. E. Taylor, and T. R. Walsh (Rutherford High Energy Laboratory, Chilton, England, 1966).
- [46] D. A. Simovici, *Linear Algebra Tools for Data Mining* (World Scientific, Singapore, 2012).
- [47] L. Campos Venuti, Z. Ma, H. Saleur, and S. Haas, *Phys. Rev. A* **96**, 053858 (2017).
- [48] L. Ge, *Phys. Rev. A* **95**, 023812 (2017).
- [49] S. Malzard, C. Poli, and H. Schomerus, *Phys. Rev. Lett.* **115**, 200402 (2015).